Title:

Nanomolar Surface-Active Charged Impurities Account for the Zeta Potential of Hydrophobic Surfaces

Author(s):

Yuki Uematsu, Douwe Jan Bonthuis, and Roland R. Netz

Citation:

"Langmuir 2020, 36, 13, 3645–3658 ; https://doi.org/10.1021/acs.langmuir.9b03795"

Nanomolar surface-active charged impurities account for the zeta potential of hydrophobic surfaces

Yuki Uematsu,[*,†,‡] Douwe Jan Bonthuis,[¶] and Roland R. Netz[§]

†*Department of Physics, Kyushu University, 819-0395 Fukuoka, Japan*

‡*Laboratoire de Physique de l'Ecole normale supérieure, ENS, Université PSL, CNRS, Sorbonne Université, Université de Paris, F-75005 Paris, France*

¶*Institute of Theoretical and Computational Physics, Graz University of Technology, 8010 Graz, Austria*

§*Fachbereich Physik, Freie Universität Berlin, 14195 Berlin, Germany*

E-mail: uematsu.yuki@phys.kyushu-u.ac.jp

Abstract

The electrification of hydrophobic surfaces is an intensely debated subject in physical chemistry. We theoretically study the ζ potential of hydrophobic surfaces for varying pH and salt concentration by solving the Poisson-Boltzmann and Stokes equations with individual ionic adsorption affinities. Using the ionic surface affinities extracted from the experimentally measured surface tension of the air-electrolyte interface, we first show that the interfacial adsorption and repulsion of small inorganic ions such as H_3O^+, OH^-, HCO_3^-, and CO_3^{2-} are irrelevant for the ζ potential observed in experiments because the surface affinities of these ions are too small. Even if we take hydrodynamic slip into account, the characteristic dependence of the ζ potential on

pH and salt concentration cannot be reproduced. Instead, to explain the sizable experimentally measured ζ potential of hydrophobic surfaces, we assume minute amounts of impurities in the water and include the impurities' acidic and basic reactions with water. We find good agreement between our predictions and the reported experimental ζ potential data of various hydrophobic surfaces. Our theory suggests that the impurities consist of a mixture of weak acids ($pK_a = 5$ to 7) and weak bases ($pK_b = 12$) at a concentration of the order of 10^{-7} M.

Introduction

The ζ potential is derived from experimentally measured electro-osmotic or electrophoretic mobilities using the Helmholtz-Smoluchowski equation and within this simple theoretical framework describes the electrostatic potential at the shear plane.[1,2] Because the ζ potential is an important and useful quantity for characterizing the properties of electrified surfaces, theoretical and experimental studies of the ζ potential have been performed for over a hundred years. For most metal oxides, such as silica,[3] aluminium oxide,[4] and titanium oxides,[4] the surface charge originates from the protonation and deprotonation of the oxide surface, and the pH determines the surface charge density by charge regulation.[5] Whereas a quantitative description of the surface charge and the ζ potential of these metal oxides is well developed, the surface charge of other surfaces is still poorly understood.

In particular, solid surfaces such as Teflon AF (amorphous fluoropolymer),[6] carbons[7–10] and boron-nitride,[11] sulfide minerals,[12–15] and silver halides[16,17] exhibit a negative ζ potential at neutral pH and an isoelectric point located around pH = 1 to 4.[18] The contact angle of water droplets at these surfaces approaches, or exceeds, 90°,[19,20] meaning that these surfaces are hydrophobic. The ζ potentials of gas bubbles[21–35] and oil droplets[36–45] show behavior very similar to these hydrophobic solid surfaces, suggesting that the electrification of solid, liquid and gaseous hydrophobic surfaces is governed by a universal mechanism. The nature of this mechanism, however, is still an open question in physics and chemistry[46–49] because

these interfaces are chemically inert, *i.e.* they do not have dissociable groups.

A widely used explanation for the puzzling observation of negative ζ potentials at hydrophobic surfaces is hydroxide ion (OH^-) adsorption,[42,50–54] because ideal purified water at neutral pH includes only hydroxide ions as anions. This explanation is supported by the potential of mean force of OH^- ions on air, graphene, and boron nitride surfaces calculated by ab-initio molecular dynamics simulations[53–56] and by surface-sensitive molecular spectroscopy.[57] However, it contradicts experimental measurements of the surface tension of NaOH solutions at the air interface, because the surface tension of a NaOH solution is higher than the surface tension of a NaCl solution of the same concentration, whereas the chloride ion (Cl^-) is usually considered to be surface-inactive.[58] This experimental finding implies that OH^- is more strongly repelled from the air-water interface than Cl^-. The same experiments show that H_3O^+ weakly absorbs onto the air interface because most acid solutions decrease the surface tension.[49,58] H_3O^+ adsorption is supported by MD simulations that predict the potential of mean force on the air surface[58–60] and surface-sensitive molecular spectroscopy.[61] Therefore, based on experimental surface tension data, if only H_3O^+ and OH^- are present in water, the ζ potential should be positive, which contradicts the experimental observations. Other explanations for the negative ζ potential suggested in the literature are polarization of the interface,[62] bicarbonate adsorption,[48] charge transfer between water molecules,[47,63] and impurity effects.[46,49,64]

Assuming a charged sphere (or capillary) with the surface potential ψ_0 immersed in an electrolyte solution, the linearized electro-hydrodynamic equations determine the electrophoretic (or electro-osmotic) mobility μ as $\mu = (\varepsilon\varepsilon_0\psi_0/\eta)f(\psi_0, \kappa R, \{\lambda_i\}, \dots)$, where ε is the dielectric constant, ε_0 is the vacuum permittivity, η is the solution viscosity, κ is the inverse of the Debye length, R is the radius of the sphere (or capillary) and λ_i is the molar conductivity of ions of type i. The function f is model-dependent, and analytical expressions are known only for limiting cases. For solid particles, $f = 1$ for the planar limit $\kappa R \to \infty$, corresponding to the Helmholtz-Smoluchowski formula,[65] while $f = 2/3$ for the point limit

$\kappa R \to 0$, which is the Hückel formula.[66] For arbitrary κR and ψ_0, f can be calculated numerically.[67,68] Note that the electrophoretic and electro-osmotic mobilities depend on the viscous properties of the interfacial layer, which is of particular importance for gas bubbles and oil droplets, where f depends on the gas or oil viscosity.[69–71]

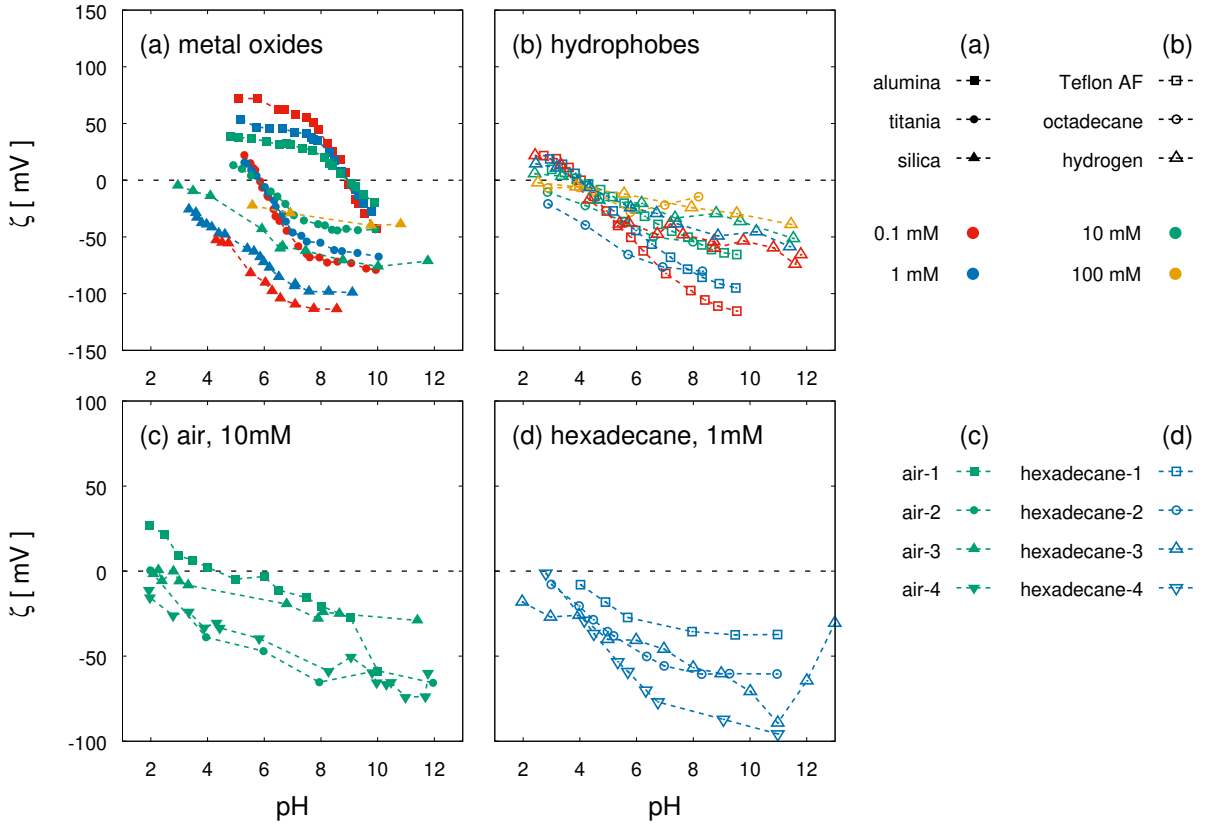

Figure 1: Collection of experimental ζ potentials of (a) metal oxides: alumina,[4] titania,[4] and silica,[3] (b) hydrophobic systems: Teflon AF surfaces,[6] octadecane droplets,[43] and hydrogen[31] and (c) air bubbles in 10 mM NaCl solution: air-1,[35] air-2,[35] air-3,[33] and air-4,[26] and (d) hexadecane droplets in 1 mM NaCl solution: hexadecane-1 and -2,[46] hexadecane-3,[45] and hexadecane-4.[41] In a and b, the colors represent different bulk salt concentrations, whereas the shapes of the symbols represent the different surface types. The broken lines are guides to the eye. More details are given in Appendix A.

In experiments, the electrophoretic mobility is measured and converted into the surface potential using a model-dependent mobility formula. Typically, the Helmholtz-Smoluchowski formula is used for this. Since the Helmholtz-Smoluchowski formula neglects ion adsorption at the surface as well as interfacial dielectric anomalies, the converted surface potential is not identical to the real surface potential. Furthermore, surface slip and the inhomogeneity

of the surface viscosity complicate the definition of the shear plane. Therefore, the converted quantity is called the ζ potential instead of surface potential. In Fig. 1ab we show a collection of experimental ζ potentials of metal oxides and different hydrophobic surfaces for different salt concentrations as a function of pH. For metal oxides, the ζ potentials decrease as the pH increases and exhibit isoelectric points where the ζ potential vanishes. The isoelectric points depend on the type of metal oxide, but are almost independent of the salt concentration. The ζ potentials of the hydrophobic systems corresponding to Teflon AF surfaces, octadecane droplets and hydrogen bubbles are plotted in Fig. 1b. They all exhibit isoelectric points around pH = 4[18] and show a similar dependence on pH and salt concentration. Naive comparison of the data in Figs. 1a and 1b would suggest that the surface charge on hydrophobic surfaces is similar to the one on silica, which is puzzling since silica has dissociable surface groups, in contrast to the hydrophobic surfaces. In Figs. 1c and 1d, we show a collection of experimental ζ potentials of air bubbles in a 10 mM NaCl solution[26,33–35] and hexadecane droplets in a 1 mM NaCl solution.[41,45,46] Even though the materials are the same, the experimental ζ potentials show a large spread, which implies that the electrification of the hydrophobic surfaces is governed by an uncontrolled factor in the experiments such as measuring techniques and protocols, methods of synthesis or purification of chemicals.

The ζ potentials of hydrophobic surfaces have been quantitatively explained by assuming OH^- adsorption.[50] The fit of that model to the experimental data yields an interfacial ionic product of the H_3O^+ and OH^- concentrations around 6,[50] which is substantially lower than the bulk value of 14. A simple calculation demonstrates that the surface adsorption energy of OH^- in this case equals $-(14-6)\ln 10 \times k_BT = -18.4k_BT$ (the minus sign means adsorption), which is even larger than the adsorption energy of typical ionic surfactants and, as mentioned above, contradicts the experimental surface tension data of bases. In fact, using experimental surface tension data and assuming an adsorption layer thickness of 0.5 nm, we have previously estimated the surface adsorption energy to be $-15.6k_BT$ for the surfactant dodecylsulfate, $+1.6k_BT$ for OH^- and $-0.9k_BT$ for H_3O^+, which means that OH^- ions are repelled from

and H_3O^+ ions are slightly attracted to the air-water interface.[72]

In this paper, we propose the presence of minute quantities of basic and acidic impurities to explain the experimental ζ potentials of hydrophobic surfaces in a way that is consistent with the ion affinities extracted from surface tension measurements. In a previous calculation, we have proposed acidic impurity effects,[49] which reproduces the correct trend of the ζ potential as a function of pH and salt concentration, as well as the Jones-Ray effect,[72,73] the disjoining pressure of the water wetting film on metal oxide surfaces,[49,74] and other features of the air-water interface.[75–78] Here, we first demonstrate that for surface affinities that are consistent with experimental electrolyte surface tension data, interfacial effects that involve water ions and dissolved CO_2 cannot explain the experimentally measured ζ potentials of hydrophobic systems even if hydrodynamic slip effects are taken into account. In a second step we introduce surface-active charged impurities in the solution and perform a detailed analysis of their effect on the ζ potential. Finally, we study the effects of the impurity concentration and the impurity pK_a and pK_b values and propose a consistent model for the experimentally measured negative ζ potential of hydrophobic surfaces.

Model

In this section, we first introduce the governing electrostatic and hydrodynamic equations for a planar surface. We construct a model to calculate the ζ potential of hydrophobic surfaces including the adsorption of water ions, salt ions and charged impurities. All surface affinities of ions are extracted from experimental surface tension data or from molecular dynamics simulations. Finally, we compare the calculated ζ potentials to experimental data on planar Teflon AF surfaces,[6] which have the advantage that it can be assumed that ions do not partition into the hydrophobic material. For oils, in contrast, both inorganic and organic ions can penetrate from the aqueous phase into the oil phase,[79] and ions naturally exist in ambient air at a concentration of $\sim 10^3\,/\mathrm{cm}^3 (\sim 10^{-17}\,\mathrm{M})$.[80]

Electrostatic and hydrodynamic equations

We consider an interface located at $z = 0$ between a hydrophobic material ($z < 0$) and an electrolyte solution ($z > 0$). Different types of mobile ions are present in the electrolyte solution, whereas we assume that no ions are present in the hydrophobic material. To obtain the ion distribution and the electrostatic potential profile, we solve the Poisson-Boltzmann equation given by[81]

$$\frac{d}{dz}\left[\varepsilon_{\perp}(z)\varepsilon_0\frac{d}{dz}\psi(z)\right] = -\rho(z) \quad \text{for} \quad z > 0, \tag{1}$$

where $\varepsilon_{\perp}(z)$ is the solution dielectric profile near the interface, ε_0 is the electric permittivity of vacuum, $\psi(z)$ is the electrostatic potential. The right hand side of eq. 1 is the charge density, which we assume to obey the Boltzmann distribution including ionic adsorption potentials $U_i(z)$,

$$\rho(z) = e\sum_i q_i c_i^{\mathrm{b}} \mathrm{e}^{-eq_i\psi(z)/k_{\mathrm{B}}T - U_i(z)}, \tag{2}$$

where e is the elementary charge, i refers to the ion type, q_i is the charge in units of e, c_i^{b} is the ion bulk concentration and $k_{\mathrm{B}}T$ is the thermal energy. When we apply an electric field E_x in tangential direction to the surface, the Stokes equation for the tangential coordinate in the absence of a pressure gradient is given by

$$\frac{d}{dz}\left[\eta_{\perp}(z)\frac{d}{dz}u_x(z)\right] + \rho(z)E_x = 0, \tag{3}$$

where $\eta_{\perp}(z)$ is the viscosity profile for the tangential shear flow, and $u_x(z)$ is the solution velocity in the tangential direction.

In order to simplify the solution of eqs. 1-3, we use box profiles for the interfacial profiles $\varepsilon_{\perp}(z)$, $U_i(z)$, and $\eta_{\perp}(z)$, the parameters of which have been previously obtained by molecular

dynamics simulation,[82]

$$\varepsilon_\perp(z) = \varepsilon + (\varepsilon_{\rm int} - \varepsilon)\theta(z - z^*) \quad (4)$$

$$U_i(z) = \alpha_i \theta(z - z^*) \quad (5)$$

$$\eta_\perp(z) = \eta + (\eta_{\rm int} - \eta)\theta(z - z^*), \quad (6)$$

where ε is the bulk dielectric constant of the solution, $\varepsilon_{\rm int}$ is the interfacial dielectric constant, α_i is the adsorption energy of an ion of type i, η is the bulk viscosity of the solution, $\eta_{\rm int}$ is the interfacial viscosity. For simplicity, the width of the interfacial layer z^* is assumed to be identical for the dielectric profile, the ionic potentials of mean force, and the viscosity profile, which is a quite realistic assumption when compared with simulation results.[82] When electrostatic interactions are neglected, the integrated surface excess of type i ions is given by $z^*(\mathrm{e}^{-\alpha_i} - 1)c_i^{\rm b}$, which is equivalent to the linear version of the Langmuir adsorption isotherm,[83] the term in front of the bulk concentration is equivalent to the adsorption coefficient.

Eq. 1 is solved with the boundary conditions $d\psi/dz|_{z=0} = 0$ and $\psi|_{z\to\infty} = 0$, which reflect the zero-charge condition at the surface and the absence of an electrostatic potential in bulk. Eq. 3 is solved with the boundary conditions $u_x|_{z=0} = 0$ and $du/dz|_{z\to\infty} = 0$, which correspond to the no-slip boundary condition at the surface and the zero-shear condition in bulk. A boundary condition with finite surface slip length is regularly used for the hydrodynamic boundary condition at hydrophobic surfaces.[84] We incorporate surface slip effects at solid surfaces by using the no-slip boundary condition at $z = 0$ together with a decreased viscosity in the interfacial layer.

In planar geometry, the electro-osmotic mobility is defined by the bulk velocity divided by the applied electric field, $\mu = u_x|_{z\to\infty}/E_x$, and the ζ potential is defined by $\zeta = -\eta\mu/\varepsilon\varepsilon_0$. From the solution of eqs. 1 and 3, the ζ potential is given by,[81]

$$\zeta = \frac{\varepsilon_{\rm int}\eta}{\varepsilon\eta_{\rm int}}\psi_0 + \left(1 - \frac{\varepsilon_{\rm int}\eta}{\varepsilon\eta_{\rm int}}\right)\psi^*, \quad (7)$$

where $\psi^* = \psi|_{z=z^*}$ and $\psi_0 = \psi|_{z=0}$. For the case $\varepsilon_\perp(z) = \varepsilon$ and $\eta_\perp(z) = \eta$, i.e. when there are no interfacial dielectric and viscosity effects, the ζ potential is identical to the surface potential, ψ_0.

Parametrization of the experimental system

KCl-HCl-KOH solutions and pH effects

In the experiments on Teflon AF surfaces,[6] KCl was used as the electrolyte and HCl and KOH were used for the adjustment of the pH. Water dissociates into H_3O^+ and OH^- ions according to the reaction

$$2H_2O \rightleftharpoons H_3O^+ + OH^-, \quad c^{\mathrm{b}}_{H_3O} c^{\mathrm{b}}_{OH} = K_w c^{\circ 2}, \tag{8}$$

with the ionic product $K_w = 10^{-14}$ and the standard concentration $c^\circ = 1\,\mathrm{M}$. In eq. 8, as well as in the following eqs. 11, 12, and 15-18, we use the ideal-gas approximation for the ion activities. Within this approximation, the pH is defined by $\mathrm{pH} = -\log_{10}(c^{\mathrm{b}}_{H_3O}/c^\circ)$.

The control parameters in the experiments are the bulk hydronium ion concentration, $c^{\mathrm{b}}_{H_3O}$, and the bulk salt concentration, $c^{\mathrm{b}}_{\mathrm{salt}}$. The hydroxide ion concentration is determined by eq. 8, but the potassium and chloride ion concentrations are normally not equal to $c^{\mathrm{b}}_{\mathrm{salt}}$ because HCl and KOH added for pH adjustment contain potassium and chloride ions. Solving the charge balance equation, we can determine the concentrations of potassium and chloride ions as follows. We define the charge-weighted sum of concentrations (excluding KCl) by $C = \sum_{i \neq \mathrm{K,Cl}} q_i c^{\mathrm{b}}_i$, by which we obtain

$$c^{\mathrm{b}}_{\mathrm{K}} = c^{\mathrm{b}}_{\mathrm{salt}}, \quad c^{\mathrm{b}}_{\mathrm{Cl}} = c^{\mathrm{b}}_{\mathrm{salt}} + C \quad \text{for} \quad C > 0, \tag{9}$$

and otherwise

$$c^{\mathrm{b}}_{\mathrm{K}} = c^{\mathrm{b}}_{\mathrm{salt}} - C, \quad c^{\mathrm{b}}_{\mathrm{Cl}} = c^{\mathrm{b}}_{\mathrm{salt}} \quad \text{for} \quad C < 0. \tag{10}$$

Eqs. 9 and 10 hold even when impurities and (bi)carbonate ions are present in the solution.

Acidic and basic impurities

Although ultrapure water was used in the experiments,[6] we assume that trace amounts of surface-active charged impurities are likely to be present in the water. We consider two kinds of impurity, AH and B. AH is an acidic impurity which is deprotonated according to

$$\mathrm{AH} + \mathrm{H_2O} \rightleftharpoons \mathrm{A^-} + \mathrm{H_3O^+}, \quad \frac{c_{\mathrm{A}}^{\mathrm{b}}}{c_{\mathrm{AH}}^{\mathrm{b}}} = 10^{\mathrm{pH}-\mathrm{pK_a}}, \tag{11}$$

where $\mathrm{K_a}$ is the acid reaction constant. B is a basic impurity which is protonated according to

$$\mathrm{B} + \mathrm{H_2O} \rightleftharpoons \mathrm{BH^+} + \mathrm{OH^-}, \quad \frac{c_{\mathrm{BH}}^{\mathrm{b}}}{c_{\mathrm{B}}^{\mathrm{b}}} = 10^{14-\mathrm{pH}-\mathrm{pK_b}}, \tag{12}$$

where $\mathrm{K_b}$ is the basic reaction constant; alternatively, the acid reaction constant $\mathrm{pK_a}$ of the protonated base equals $14 - \mathrm{pK_b}$. The impurities are assumed to be surface-active and the total concentrations of acids and bases, defined by

$$c_{\mathrm{A,tot}}^{\mathrm{b}} = c_{\mathrm{A}}^{\mathrm{b}} + c_{\mathrm{AH}}^{\mathrm{b}}, \tag{13}$$

and

$$c_{\mathrm{B,tot}}^{\mathrm{b}} = c_{\mathrm{B}}^{\mathrm{b}} + c_{\mathrm{BH}}^{\mathrm{b}}, \tag{14}$$

respectively, are used as the adjustable model parameters.

Dissolution of carbon dioxides

Because the Teflon AF experiments were performed using degassed ultrapure water under nitrogen atmosphere,[6] we do not need to consider the dissolution of carbon dioxide. However, other experiments have been done in ambient air conditions,[31] and therefore we also treat the effect of $\mathrm{CO_2}$ dissolution. When water is in equilibrium with the ambient atmosphere,

carbon dioxide dissolves into the water according to the reaction

$$\mathrm{CO_{2(gas)}} \rightleftharpoons \mathrm{CO_{2(aq)}}, \quad \mathrm{H_{cc}} = \frac{c^{\mathrm{b}}_{\mathrm{CO_2}}}{c^{\mathrm{air}}_{\mathrm{CO_2}}}, \tag{15}$$

where the Henry constant is given by $\mathrm{H_{cc}} = 0.86$ and the ambient concentration of CO_2 is given by $c^{\mathrm{air}}_{\mathrm{CO_2}} = 1.6 \times 10^{-5}\,\mathrm{M}$.[85] The dissolved CO_2 reacts with the water according to the following reactions

$$\mathrm{CO_{2(aq)}} + \mathrm{H_2O} \rightleftharpoons \mathrm{H_2CO_{3(aq)}}, \quad \frac{c^{\mathrm{b}}_{\mathrm{H_2CO_3}}}{c^{\mathrm{b}}_{\mathrm{CO_2}}} = \mathrm{K_{CO_2}}, \tag{16}$$

$$\begin{gathered}\mathrm{H_2CO_{3(aq)}} + \mathrm{H_2O} \rightleftharpoons \mathrm{HCO_3^-} + \mathrm{H_3O^+}, \\ \frac{c^{\mathrm{b}}_{\mathrm{HCO_3}} c^{\mathrm{b}}_{\mathrm{H_3O}}}{c^{\mathrm{b}}_{\mathrm{H_2CO_3}}} = \mathrm{K_{H_2CO_3}} c^{\circ},\end{gathered} \tag{17}$$

$$\begin{gathered}\mathrm{HCO_3^-} + \mathrm{H_2O} \rightleftharpoons \mathrm{CO_3^{2-}} + \mathrm{H_3O^+}, \\ \frac{c^{\mathrm{b}}_{\mathrm{CO_3}} c^{\mathrm{b}}_{\mathrm{H_3O}}}{c^{\mathrm{b}}_{\mathrm{HCO_3}}} = \mathrm{K_{HCO_3}} c^{\circ},\end{gathered} \tag{18}$$

where the equilibrium constants are $\mathrm{K_{CO_2}} = 2.6 \times 10^{-3}$, $\mathrm{K_{H_2CO_3}} = 1.7 \times 10^{-4}$, and $\mathrm{K_{HCO_3}} = 4.7 \times 10^{-11}$.[85] The pH of water with dissolved CO_2 follows as pH = 5.6 using the chemical equilibrium eqs. 8 and 15-18, which agrees well with the experimental pH of aqueous solutions that are in contact with ambient air.[74,85]

Interfacial properties

For a hydrophobic diamond surface, we have previously determined $\varepsilon_{\mathrm{int}}/z^* = 8.3\,/\mathrm{nm}$[86] and a slip length of $b = 2.1\,\mathrm{nm}$ (with $\eta_{\mathrm{int}} = \eta$)[87] from molecular dynamics simulations. Fixing $z^* = 0.5\,\mathrm{nm}$, we obtain from these values $\varepsilon_{\mathrm{int}} = 4.2$ and $\eta_{\mathrm{int}}/\eta = 0.2$ (assuming vanishing surface slip, $b = 0$). For Cl^- and Na^+, we have determined $\alpha_{\mathrm{Cl}} = 1.0$ and $\alpha_{\mathrm{Na}} = 1.2$ by integrating the potential of mean force obtained by molecular dynamics simulation.[88] All other α_i values are determined by fitting the experimental air-water surface tension using

the present model with $\varepsilon_{\text{int}} = \varepsilon$ (see Appendix B where we determine the surface affinities of carbonate ions).[49,72] Regarding the interfacial viscosity, we consider $\eta_{\text{int}} \neq \eta$ only in section III.A.1 and Appendix C, and otherwise $\eta_{\text{int}} = \eta$. Since the effect of a modified interfacial dielectric constant is not significant at small surface charge density, as shown in Appendix D, we use $\varepsilon_{\text{int}} = \varepsilon$ in the main text. The surface affinities for A^- and BH^+ are for concreteness taken from dodecylsulfate and dodecyldimethylammonium data, without implying any specific identities of the impurities. The surface affinities of all ions are shown in Table 1.

Table 1: Ion-specific surface affinities to the air-water interface.

Ion	α_i	Ref.
H_3O^+	-0.9	72
OH^-	1.6	72
HCO_3^-	-0.4	72
CO_3^{2-}	1.4	Appendix B
Na^+	1.2	72, 88
K^+	1.2	49
Cl^-	1.0	72, 88
A^-	-15.6	72
BH^+	-14.5	72

Results and discussion

In this section, we solve the model described in the last section and present the ζ potential for varying pH and bulk salt concentration. We also investigate the effects of CO_2 dissolution, slip, and the presence of impurities. First, we solve the chemical equilibrium equations for all ions, eqs. 8 to 18, and determine the bulk concentration of each ion type. Then, we solve the Poisson-Boltzmann equation (eq. 1) using the analytic solutions for monovalent ion species.[81] When we consider divalent CO_3^{2-} originating from CO_2 dissolution, we employ a numerical solution of eq. 1. To calculate the ζ potential, we do not need to solve the Stokes equation (eq. 3), but substitute ψ_0 and ψ^* into eq. 7.

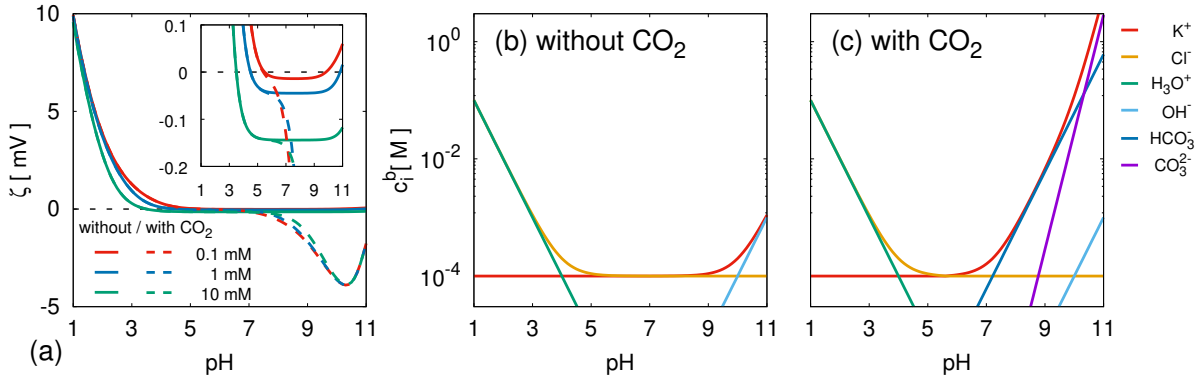

Figure 2: (a) ζ potential of the hydrophobe-KCl solution interface as a function of pH calculated with (broken lines) and without (solid lines) CO_2-dissolution effects. The inset shows a magnification. We use $T = 298\,\mathrm{K}$, $z^* = 0.5\,\mathrm{nm}$, $\varepsilon_{\mathrm{int}} = \varepsilon = 78$, $\eta_{\mathrm{int}} = \eta$, and all α_i are summarized in table. 1. (b) Plot of the ion bulk concentrations as a function of pH for the 0.1 mM KCl solution without CO_2. (c) Plot of the ion bulk concentrations as a function of pH for the 0.1 mM KCl solution with CO_2.

In the absence of impurities

First, we calculate the ζ potential of the hydrophobe-electrolyte interface without impurities. We demonstrate that even if we include CO_2 dissolution and surface slip, the theory cannot reproduce the experimentally measured ζ potentials. Note that we extract the surface affinities of the ions from experimentally measured electrolyte surface tensions and thus use a model for electrified electrolyte interfaces that is consistent with all available experimental data.

Fig. 2a shows the ζ potential of a hydrophobe-KCl solution interface without impurities as a function of pH. The solid lines include only the water dissociation according to eq. 1, whereas the broken lines include CO_2 dissolution according to eqs. 15-18 as well as water dissociation. In Fig. 2bc the bulk ion concentrations are plotted as a function of pH for fixed $c^{\mathrm{b}}_{\mathrm{salt}} = 0.1\,\mathrm{mM}$ with/without CO_2, which follow from solving the chemical reaction eqs. 8-10 and 15-18.

Both with and without CO_2 dissolution, the ζ potentials are in the range of $-5\,\mathrm{mV} < \psi_0 < 10\,\mathrm{mV}$, which is much smaller than the magnitude of the ζ potentials measured in experiments. For a 0.1 mM KCl solution without CO_2, the main bulk ionic components for

acidic conditions (pH < 4) are H_3O^+ and Cl^-, as shown in Fig. 2b. Because the interface affinity of H_3O^+ is more pronounced than the interface affinity of Cl^-, $\alpha_{H_3O} < \alpha_{Cl}$, the ζ potential for acidic conditions is positive. At neutral pH ($4 <$ pH < 10), the main bulk ionic components are K^+ and Cl^-, and thus, the ζ potential is slightly negative because $\alpha_K > \alpha_{Cl}$. For basic conditions (pH > 10), the main bulk ionic components are K^+ and OH^-. Because $\alpha_K < \alpha_{OH}$, the ζ potential is again positive.

For a 0.1 mM KCl solution in the presence of CO_2, the main ionic components vary with pH. For pH < 4 and $4 <$ pH < 7, the main ionic components in bulk are the same as those without CO_2, whereas for $7 <$ pH < 10, K^+ and HCO_3^- are the main ionic components in bulk, and thus, the ζ potential becomes negative because $\alpha_K > \alpha_{HCO_3}$. For pH > 10, the contribution of CO_3^{2-} becomes important, and the ζ potential is mostly negative but increases rapidly for very large pH.

These results suggest that in order to reproduce ζ potentials of magnitude similar to the experimental values, which are around -50 mV, it is necessary to assume the presence of charged components with very large surface affinities.

Effect of hydrodynamic slip

Interfacial slip, which in our model is equivalent to the presence of an interfacial layer with a low viscosity, enhances the ζ potential. Fig. 3 shows the ζ potential of KCl solutions in the presence of slip. We use an interfacial viscosity $\eta_{int} = 0.2\eta$ in Fig. 3a and $\eta_{int} = 0.05\eta$ in Fig. 3b. The corresponding slip lengths are given by, respectively, $b = z^*(\eta/\eta_{int} - 1) = 2$ nm, which is identical to the slip length found for hydrophobic diamond surfaces in molecular dynamics simulations,[87] and $b = 9.5$ nm.[6] The results in Fig. 3 show that slip enhances the ζ potential but does not change the pH dependence of the curves as long as η_{int} is independent of pH. Comparing the calculated curves with the experimental data, both with and without CO_2, one sees that the pH dependence does not agree with the experimental data. In addition, the slip length $b = 9.5$ nm used in Fig. 3b is very large compared to typical slip

lengths obtained in molecular dynamics simulations of hydrophobic surfaces.[89] In Appendix D we furthermore demonstrate that interfacial dielectric effects do not significantly modify the ζ potential of hydrophobic surfaces.

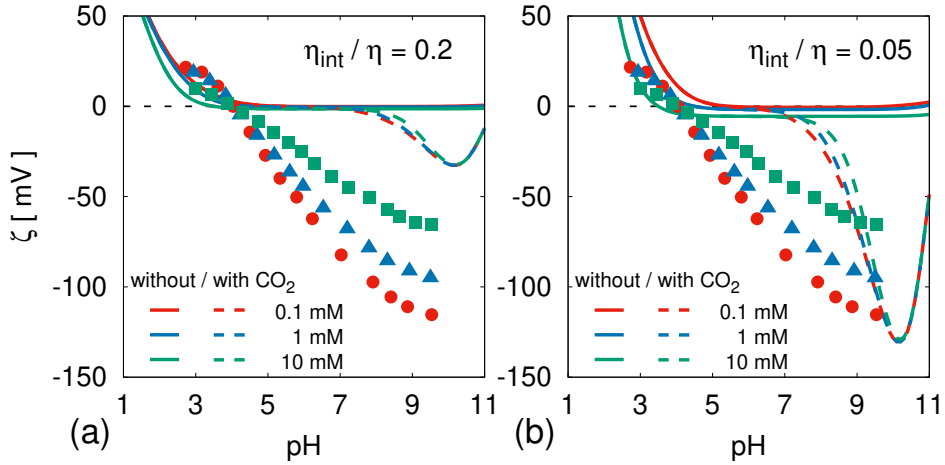

Figure 3: Effect of slip on the ζ potential of the hydrophobe-KCl solution interface as a function of pH, calculated with (broken lines) and without (solid lines) CO_2. The interfacial viscosity is set to (a) $\eta_{\rm int}/\eta = 0.2$, corresponding to a slip length of $b = z^*(\eta/\eta_{\rm int} - 1) = 2\,{\rm nm}$, and to (b) $\eta_{\rm int}/\eta = 0.05$, corresponding to a slip length of $b = z^*(\eta/\eta_{\rm int} - 1) = 9.5\,{\rm nm}$. Other parameters are the same as those used in Fig. 2. The symbols represent the experimental data for Teflon AF surfaces.[6]

In the presence of impurities

Because the effect of slip is not sufficient to explain the pH dependence of the experimental ζ potential, we consider the presence of impurities.[46,72] Specifically, we consider the effect of acidic and basic surface-active impurities that are present in water as well as the effect of surface-active anionic impurities that are present in the KOH solution added for adjustment of the pH. For simplicity we do not consider the presence of CO_2 nor the effects of slip in the remainder of the paper.

Acidic surface-active impurities in water

We use the ionic affinity for acidic impurities $\alpha_{\rm A} = -15.6$ which is extracted from the experimental surface tension of the interface between sodium dodecylsulfate solution and

air.[72] Fig. 4 shows the comparison between the experimental and theoretical ζ potentials for acidic impurity concentrations $c^{\mathrm{b}}_{\mathrm{A,tot}} = 50\,\mathrm{nM}$ and $500\,\mathrm{nM}$. We use $\mathrm{pK_a} = 5$ (broken lines), which is the value typical for the carboxyl acid group, and $\mathrm{pK_a} = 7$ (solid lines), which describes the experimental data better. In fact, the deprotonated impurity species dominates the surface charge of the hydrophobic interface. For impurity concentration $c^{\mathrm{b}}_{\mathrm{A,tot}} = 500\,\mathrm{nM}$ with $\mathrm{pK_a} = 7$ the experimental Teflon AF ζ potential data are described quite well.

Figure 5 displays the $\mathrm{pK_a}$ and $\mathrm{pK_b}$ values of typical acidic and basic groups that are present in surfactant molecules.[90] The most ubiquitous acids in nature are carboxylic acids with a bulk $\mathrm{pK_a}$ around 5,[90] which is in fact equal to the $\mathrm{pK_a}$ found by fitting a similar impurity model to hexadecane data.[46] The fact that our best fit $\mathrm{pK_a} = 7$ is slightly higher may be specific to the experimental conditions or reflect a shift of the $\mathrm{pK_a}$, which in fact is expected for acidic groups that are close to low-dielectric surfaces.[91]

The slip effect on the impurity-induced ζ potential is considered in Appendix C. There we show that using $b = z^*(\eta/\eta_{\mathrm{int}} - 1) = 2\,\mathrm{nm}$, which is identical to the slip length found for hydrophobic diamond surfaces in molecular dynamics simulations,[87] we cannot obtain a value for $c^{\mathrm{b}}_{\mathrm{A,tot}}$ that reproduces the experimental data. Interfacial dielectric effects reduce the fitted impurity concentration by $\sim 40\%$, as shown in Appendix D, which is insignificant in the context of the present study.

Basic surface-active impurities in water

In strongly acidic conditions the experimental data exhibit positive ζ potentials which cannot be reproduced with acidic impurities and which suggests the additional presence of basic impurities. For the surface affinity of the basic impurity species we use the value $\alpha_{\mathrm{BH}} = -14.5$, which was previously extracted from the experimental surface tension of dodecyldimethylammonium chloride solutions.[72] Since the parameters $c^{\mathrm{b}}_{\mathrm{A,tot}} = 500\,\mathrm{nM}$ and $\mathrm{pK_a} = 7$ for the acidic impurity species accurately describe the experimental ζ potential data in the pH range of $4 < \mathrm{pH} < 8$, we do not change these parameters in the following analysis.

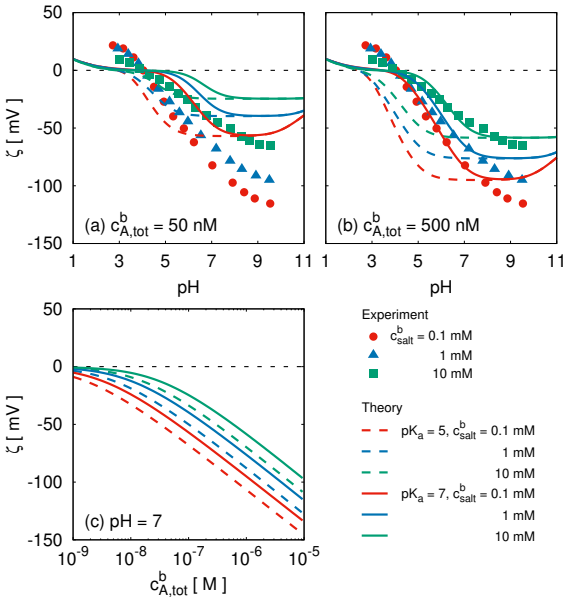

Figure 4: (a,b) Effects of acidic impurities on the ζ potential as a function of pH for $pK_a = 7$ (solid lines) and for $pK_a = 5$ (broken lines). (c) ζ potential as a function of $c^b_{A,tot}$. The symbols in (a,b) represent the experimental data.[6] The parameters are the same as those used in Fig. 2 and all α_i are summarized in table 1.

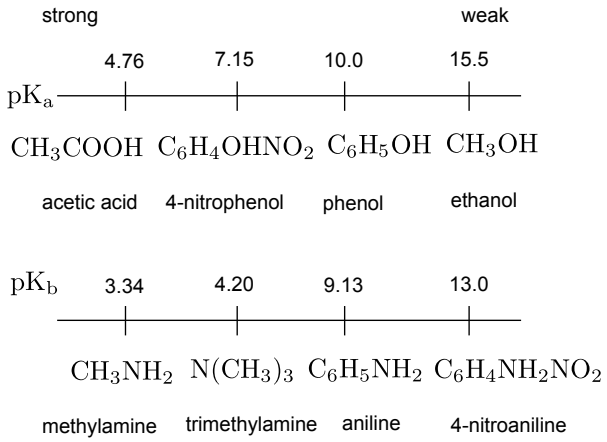

Figure 5: Collection of a few pK_a and pK_b values for typical acidic and basic groups.[90]

Fig. 6 shows the effect of basic impurities on the ζ potential for $\mathrm{pK_b} = 12$ (solid lines) and $\mathrm{pK_b} = 4$ (broken lines). Typical bases such as fatty primary amines have $\mathrm{pK_b}$ values around 4,[90] but such a value leads to neutralization of deprotonated acidic impurities at the interface and bad agreement with the experimental data, as seen in Fig. 6. We find good agreement between experiment and theory for a basic impurity concentration $c^{\mathrm{b}}_{\mathrm{B,tot}} = 600\,\mathrm{nM}$ and $\mathrm{pK_b} = 12$. The value $\mathrm{pK_b} = 12$ indicates a very weak base which is only half protonated even at a low pH of pH = 2. Figure 5 shows that bases that have such a low $\mathrm{pK_b}$ do in fact exist, but their presence will depend on the specific experimental conditions.

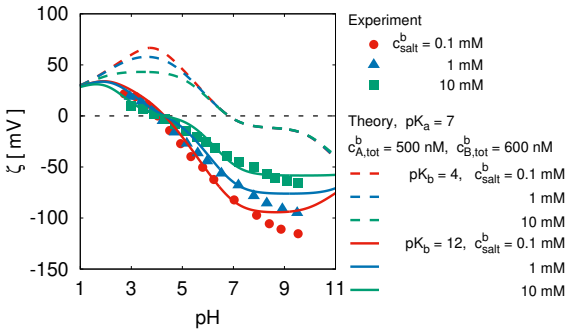

Figure 6: The effect of additional basic impurities on the ζ potential as a function of pH. The symbols represent the experimental ζ potential of Teflon AF,[6] whereas the lines depict the theoretical ζ potential. Impurities with $\mathrm{pK_b} = 4$ (strong base, broken lines) and 12 (weak base, solid lines) are examined. The parameters are the same as those used in Fig. 2 and all α_i are summarized in table 1.

Negatively charged surface-active impurities in KOH

Although the solid lines in Fig. 6 are in good agreement with the experimental data for most values of the pH, there is still a discrepancy for strongly basic conditions (pH > 8). We demonstrate next that this small discrepancy can be eliminated by additionally assuming the presence of an acidic surface-active impurity in KOH. The rationale behind this assumption is that alkali hydroxides are strongly hygroscopic and cannot be purified by roasting, which makes it difficult to keep them pure. We implement the presence of impurities in KOH by modifying the total acid impurity concentration according to $\tilde{c}^{\mathrm{b}}_{\mathrm{A,tot}} = c^{\mathrm{b}}_{\mathrm{A,tot}} + \nu c^{\mathrm{b}}_{\mathrm{OH}}$, where ν is the ratio of $\mathrm{OH^-}$ to $\mathrm{A^-}$ in KOH salts and therefore is a measure of the fraction of impurities

in KOH. For simplicity, we use the same surface affinity and the same pK_a for the impurity that is present in KOH as for the acidic impurity that is present in water.

Fig. 7 shows the effect of an impurity present in KOH. The broken lines are the same as the solid lines in Fig. 6, and thus, they are calculated without an impurity in KOH. The solid lines are calculated in the presence of an impurity in KOH using the impurity fraction $\nu = 0.05$. From the comparison with the experimental data we see that in the presence of an impurity in KOH good agreement between theory and experiment is achieved also in strongly basic conditions.

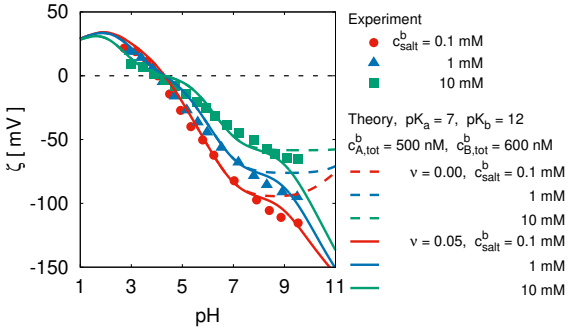

Figure 7: Effect of an additional impurity present in KOH on the ζ potential. The broken lines are calculated without an impurity in KOH, whereas the solid lines account for an impurity in KOH. We use the impurity fraction $\nu = 0.05$ for the ratio of A^- to OH^- in KOH salts. The impurity species in KOH has the same pK_a value and the same surface affinity as the acidic impurity present in water. Other parameters are the same as those used in Fig. 2 and all α_i are summarized in table 1. The symbols represent the experimental data for Teflon AF surfaces.[6]

Two kinds of acidic impurities in the water

Accurate fits to the experimental data can also be achieved without assuming impurities in the added KOH, by taking more types of water impurities into account instead. We consider the effect of a second acidic impurity in water with a different pK_a value. Keeping a basic impurity with $c^b_{B,tot} = 600\,nM$ and $pK_b = 12$ and the first acidic impurity A_1^- parameters at $c^{b,tot}_{A_1} = 500\,nM$ and $pK_{a1} = 7$, we introduce a second acidic impurity A_2^- which is characterized by a bulk concentration $c^b_{A_2,tot}$ and a value pK_{a2}. The broken lines in Fig. 8 include only one kind of acidic impurity, whereas the solid lines include two different

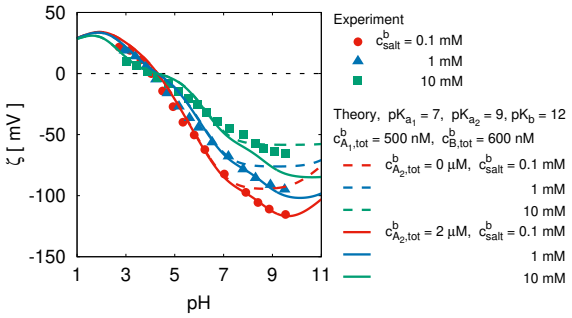

Figure 8: Effect of the presence of a second acidic impurity on the ζ potential. The broken lines are predictions without a second acidic impurity species, whereas the solid lines are predictions in the presence of a second acidic impurity species. Keeping $c^{\rm b}_{\rm A_1,tot} = 500\,{\rm nM}$, $pK_{a1} = 7$, $\alpha_{\rm A_1} = -15.6$, as well as $c^{\rm b}_{\rm B,tot} = 600\,{\rm nM}$, $pK_b = 12$, $\alpha_{\rm BH} = -14.5$, we use $c^{\rm b}_{\rm A_2,tot} = 2\,\mu{\rm M}$, $\alpha_{\rm A_2} = -15.6$, and $pK_{a2} = 9$. Other parameters are the same as those used in Fig. 2. The symbols represent the experimental data for Teflon AF surfaces.[6]

acidic impurities with $pK_{a1} = 7$ and $pK_{a2} = 9$. A fit to the experimental $c^{\rm b}_{\rm salt} = 0.1\,{\rm mM}$ data (red circles) in the basic pH range yields $c^{\rm b}_{\rm A_2,tot} = 2\,\mu{\rm M}$. We see that with a second impurity we obtain good agreement between theory and experimental data even in basic conditions and without assuming the presence of impurities in the added KOH.

What is responsible for the negative ζ potential of hydrophobic surfaces?

In the previous sections, we have demonstrated that water ions and dissolved CO_2 cannot explain the experimentally measured negative ζ potential of hydrophobic surfaces. We then proceeded to discuss the effects of various impurities on the ζ potential of hydrophobic surfaces. Our results suggest that the ζ potential of hydrophobic surfaces originates from surface-active charged impurities that are present in the water and possibly also in the salts used for adjusting the pH. We show that the experimental data for Teflon AF surfaces can be reproduced quite well if we assume the presence of acidic impurities ($pK_a = 7$) with surface affinity $\alpha_{\rm A} = -15.6$ at a concentration of $c^{\rm b}_{\rm A,tot} = 500\,{\rm nM}$. The agreement with the experimental data at low pH is improved if we additionally assume the presence of basic impurities ($pK_b = 12$) with surface affinity $\alpha_{\rm BH} = -14.5$ at a concentration of

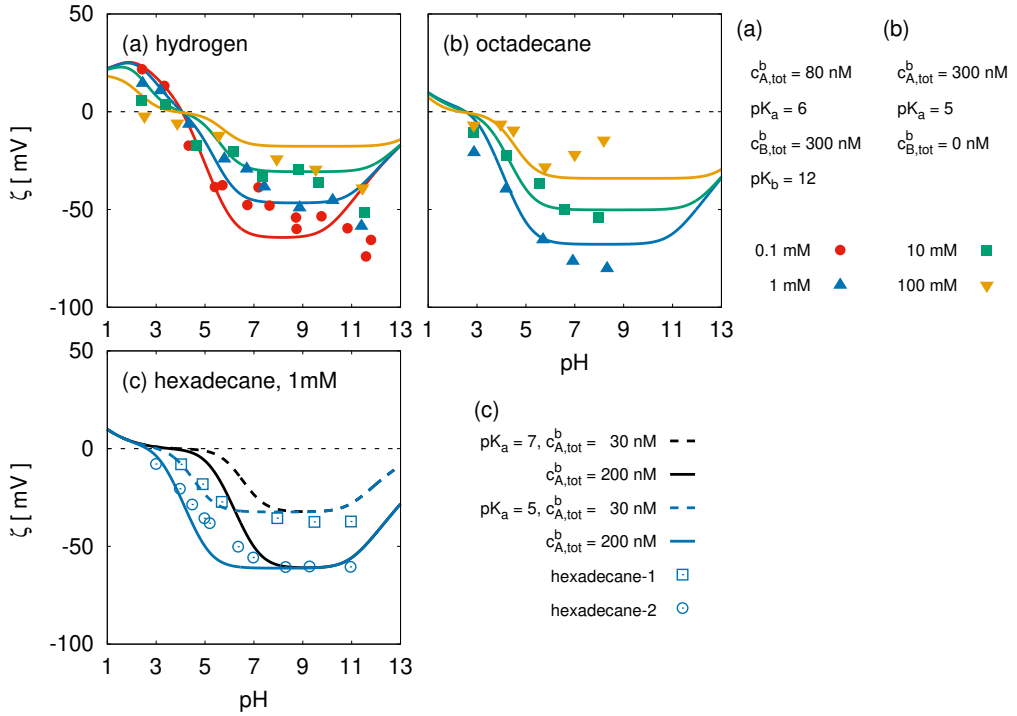

Figure 9: Comparison between theory and experimental data for (a) hydrogen bubbles,[31] (b) octadecane droplets,[43] and (c) hexadecane droplets[46] in 1mM NaCl solution. Acidic impurities $c^{\mathrm{b}}_{\mathrm{A,tot}} = 80\,\mathrm{nM}$ with $\mathrm{pK_a} = 6$ are used for the theoretical modeling in (a) and $c^{\mathrm{b}}_{\mathrm{A,tot}} = 300\,\mathrm{nM}$ with $\mathrm{pK_a} = 5$ are used in (b). In (c) acidic impurities at concentration $c^{\mathrm{b}}_{\mathrm{A,tot}} = 30\,\mathrm{nM}$ (broken lines) and $200\,\mathrm{nM}$ (solid lines) are used with $\mathrm{pK_a} = 5$ (blue) and 7 (black). Basic impurities $c^{\mathrm{b}}_{\mathrm{B,tot}} = 300\,\mathrm{nM}$ with $\mathrm{pK_b} = 12$ are used in (a). Since the data do not extend to low pH values we set $c^{\mathrm{b}}_{\mathrm{B,tot}} = 0\,\mathrm{nM}$ in (b) and (c). Other parameters are the same as those used in Fig. 4. Slip effects, interfacial dielectric effects and dissolution of carbon dioxide are not considered.

$c^{\mathrm{b}}_{\mathrm{B,tot}} = 600\,\mathrm{nM}$. Since the carbon number of dodecylsulfate is 12, a simple estimate of the adsorption energy per number of carbons gives $-15.6 k_{\mathrm{B}}T/12 = -1.3 k_{\mathrm{B}}T$. If the carbon number of the impurity's alkyl chains increases by 2, the impurity concentration needed to produce a certain ζ potential reduces approximately by a factor of 10, because $\mathrm{e}^{2.6} \approx 13$. Conversely, if the impurities have shorter alkyl chains the concentration needed to produce a certain ζ potential becomes larger. Therefore, our estimate for the impurity concentration of the order of 100 nM is only an example, and it is possible that significantly smaller impurity concentrations cause the ζ potential of hydrophobic surfaces because we do not know the chemical nature of the impurity and therefore cannot characterize precisely its surface affinity.

The ultrapure water standard, for example, Milli-Q ultrapure water, prescribes a resistivity of at least 18.2 MΩ·cm and a total organic carbon (TOC) concentration of at most 5 μg/L. In terms of concentrations, this conductivity corresponds to approximately 100 nM of charged impurities while this TOC equals 5 μg/L= 420 nM in carbon, and 35 nM in dodecylsulfate. That means that ultrapure water already includes impurities at concentrations of a few tens of nano-molar. In addition, when electrophoretic or electro-osmotic mobilities are measured, there are several possibilities of how water can be contaminated further, including contamination due to storage of water in plastic or glass containers[92] or contamination due to contact with the ambient atmosphere.[93] Charged impurities in ultrapure water have indeed been detected by mass spectrometry and liquid chromatography.[92–95]

Regarding our extracted $\mathrm{pK_a}$ and $\mathrm{pK_b}$ values, the fitted value $\mathrm{pK_a} = 7$ is substantially larger than the literature value of carboxylic acids $\mathrm{pK_a} = 5$, which is expected for acidic groups that are close to low-dielectric surfaces.[91] We also note that the experimental isoelectric points extracted from ζ potential measurements vary substantially in the range pH = 1 to 4, depending on the data set.[18] In Fig. 9a and b we show a comparison of our model predictions with hydrogen bubble[31] and octadecane[43] data, respectively. For the hydrogen bubble data, 80 nM acidic impurities with $\mathrm{pK_a} = 6$ and 300 nM basic impurities with $\mathrm{pK_b} = 12$ give good agreement. For the octadecane data, 300 nM acidic impurities with $\mathrm{pK_a} = 5$ fit

the data quite well, here basic impurities are not needed to describe the data because the octadecane data do not extend to small pH values. In Fig. 9c two different hexadecane droplet data sets[46] are compared with theoretical predictions using 30 nM and 200 nM acidic impurities with $pK_a = 5$ (blue broken and solid lines). The predictions using $pK_a = 7$ (black broken and solid lines) clearly disagree with the experimental data. In fact, a similar impurity model using $pK_a = 5$ was previously shown to describe the experimental data,[46] and it was suggested that acidic impurities originate from hexadecane because different grades of purity were used: 99.8 % (hexadecane-1, open squares) and 99 % (hexadecane-2, open circles). In this scenario, the impurities (presumably fatty acids) dissolve in both the oil and the water phase. Alternatively, it is possible that hydrophobic surfaces exhibit immobile ionic impurities. For example, the ζ potential of polymethylmethacrylate (PMMA) particles is believed to be governed by ionic end-groups of the polymers.[96] Summarizing, because it is likely that different experiments contain different combinations of impurities, the spread of pK_a values is rather plausible.

For the basic impurity, the fitted $pK_b = 12$ corresponds to a very weak base. Since the most ubiquitous base, ammonium, has a strong basic reaction constant, $pK_b = 4$, this suggests that the basic impurity is not a derivative of ammonium. Instead, the basic impurity could be a fatty alcohol,[97] an ester,[98] an ether,[98] or an acid,[99] because the oxygen atom in these molecules is only protonated in strongly acidic conditions. It is known that a dilute alcohol in water is more basic than water,[97,98] for example, isopropanol in 1M sulfuric acid has a basic reaction constant of $pK_b = 13.7$, which is close to our estimate for the basic impurity reaction constant.[97] In fact, Teflon AF is a copolymer of tetrafluoroethylene (C_2F_4) and 2,2-bis(trifluoromethyl)-4,5-difluoro-1,3-dioxole ($C_5F_8O_2$), and the ratio of the two monomers is $C_2F_4 : C_5F_8O_2 = 1 : 2$.[6] Therefore, many ether bonds ($-COC-$) exist on the surface, which in principle could act as a weak base.[98] On the other hand, the hydrogen data also suggest the presence of basic impurities. In fact, hydrogen bubbles are produced by electrolysis of water,[31] which provides a possible source of contamination with basic impurities.

For the experimentally observed enhancement of the ζ potential at large pH, we propose two scenarios: a negatively charged impurity present in the salt used to adjust the pH, or a second acidic impurity with a different pK_a value present in the water. Both scenarios are likely to occur in typical experimental conditions. In practice, impurities that are present in experiments will presumably consist of many different types of chemicals, and they will exhibit a spectrum of surface affinities, different bulk concentrations, and different pK_a and pK_b values. Even the mass spectrum of ultrapure water shows many peaks,[93,94] the origin of which are not very clear at present. Monitoring impurity distributions of pure water while measuring the ζ potential of hydrophobic surfaces at the same time would be highly desirable in future experiments.

Conclusions

We calculate the ζ potential of hydrophobic surfaces as a function of pH and salt concentration by solving the Poisson-Boltzmann and hydrodynamic equations including ion adsorption, where the ionic surface affinities have been extracted independently from surface-tension data at the air-electrolyte interface. The interface adsorption and repulsion of small inorganic ions such as H_3O^+, OH^-, HCO_3^-, and CO_3^{2-} are not sufficient to reproduce the ζ potential observed in experiments because their affinities for hydrophobic surfaces are small – of the order of $|\alpha_i| \approx 1$. The presence of hydrodynamic surface slip also is not sufficient to produce agreement with experimental ζ potential data. However, when we introduce a small amount of charged surface-active impurities in the water, we find good agreement between our calculations and the literature experimental data for Teflon AF surfaces[6] if the impurity acid and basic reaction constants are suitably chosen. Our comparison with experimental data suggests that the dominant impurity type is a weak acid with $pK_a = 5$ to 7, in order to reproduce the experimental ζ potentials at very low pH additionally a weak base with $pK_b = 12$ at concentrations of a few hundred nano-molar is needed.

We do not know the identity of the impurities, but we presume that at hydrophobic surfaces, many different types of surface active impurities can be found in addition to water ions, bicarbonate and carbonate ions. Even though the assumed bulk concentration of the impurities is only nano-molar, they accumulate at a hydrophobic surface because of their amphiphilic nature. The experimentally measured ζ potential at hydrophobic surfaces will reflect the distribution of pK_a and pK_b values of the impurities. Regarding the origin of the impurities, we consider different possibilities such as impurities in the water, contaminations from experimental processes, as well as contaminations present in added salts, acids, bases, gaseous phases, oil phases,[46] and on hydrophobic surfaces.[96] The variety of possible contamination sources can easily explain that even in nominally identical systems the ζ potentials exhibit a significant spread as shown in Fig. 1cd. Given the almost undetectably small amounts of impurities necessary to reproduce the experimentally observed ζ potential effects, it will be difficult to produce a positive proof that impurities are in fact responsible for the nonzero ζ potentials of hydrophobic solutes. Our findings thus merely suggest one possible scenario that explains the ζ potentials of hydrophobic surfaces over a large range of pH values and salt concentrations. It is crucial to realize, though, that the present theory is consistent with experimental and theoretical work on electrolyte surface tensions,[58] the Jones-Ray effect,[72,73] the disjoining pressure of wetting water films on silica[49,74] and experimental investigations of the hydrodynamic boundary conditions at air-water interfaces.[75–78]

Appendix A: Detailed description of Fig. 1

In Fig. 1 a and b, the colors represent different bulk salt concentrations, whereas the shapes of the symbols represent different surface types. Filled squares correspond to alumina (γ-Al_2O_3) powders with radius $R = 45$ to $50\,\mathrm{nm}$ in KNO_3-HNO_3-KOH solution and the conversion into the ζ potential follows Ref. 100.[4] The filled circles correspond to titania (TiO_2, rutile) powders with radius $R = 45\,\mathrm{nm}$ in KNO_3-HNO_3-KOH solution and the conversion into the ζ

potential follows Ref. 100.[4] The filled triangles correspond to planar fused silica (SiO_2) in KCl solution where acid and base are not specified and streaming current measurements are used for determining the electro-osmotic mobility (i.e. $f = -1$).[3] The open squares correspond to planar Teflon AF (poly(tetrafluoroethylene-co-2,2-bis(trifluoromethyl)-4,5-difluoro-1,3-dioxole) ($(C_2F_4)_n(C_5F_8O_2)_m$) in KCl-HCl-KOH solution where streaming current measurements are used for determining the electro-osmotic mobility.[6] The open circles correspond to octadecane ($C_{18}H_{38}$) droplets with radius $R = 150\,\mathrm{nm}$ in NaCl solution where acid and base are not specified and $f = 1$ is used for conversion.[43] The open triangles correspond to hydrogen bubbles with radius $R = 10$ to $70\,\mu\mathrm{m}$ in NaCl-HCl-NaOH solution and $f = 1$ for conversion.[31]

In Fig. 1 c and d, the shapes of the symbols represent the different experimental results on the same materials. The broken lines are guides to the eye. All data in c and d are measured in NaCl-HCl-NaOH solution. The filled squares correspond to air bubbles with sub-micrometer diameters in a 10 mM solution and $f = 1$ for conversion.[35] The filled circles correspond to air bubbles with diameters of a few tens of micrometers and $f = 1$ for conversion.[34] The filled up-pointing triangles correspond to $R = 290\,\mathrm{nm}$, where Henry's function[67] is used for conversion.[33] The filled down-pointing triangles correspond to $R = 5\,\mu\mathrm{m}$ and f for conversion is not specified.[26] The open squares and circles correspond to hexadecane droplets in a 1 mM solution with the diameter $2R = 150 - 200\,\mathrm{nm}$ and $f = 1$ for conversion, whereas the purity of hexadecane is different between squares (99.8%) and circles (99%).[46] The open up-pointing triangles correspond to diameters of about 300 nm and $f = 1$ for conversion.[33] The open down-pointing triangles correspond to diameters $3 - 8\,\mu\mathrm{m}$ and $f = 1$ for conversion.[41]

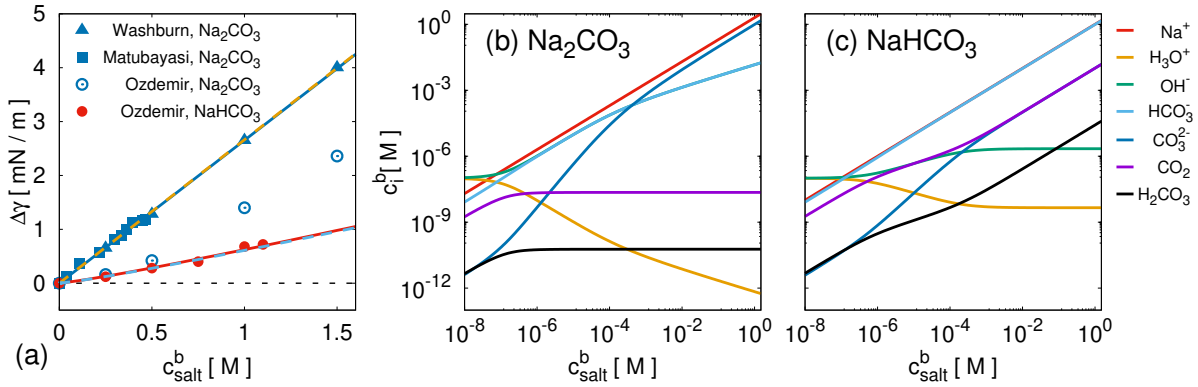

Figure 10: (a) Comparison of experimental and theoretical surface tensions of $NaHCO_3$ and Na_2CO_3 solutions. The symbols represent the experimental data,[101–103] whereas the lines are theoretical predictions. The blue and red solid lines are the calculations including the reactions eqs. 8 and 16-18. The orange and light blue broken lines are the calculation considering only the reactions $Na_2CO_3 \rightarrow 2Na^+ + CO_3^{2-}$ or $NaHCO_3 \rightarrow Na^+ + HCO_3^-$, without the reactions eqs. 8 and 16-18. We use $T = 298\,\mathrm{K}$, $z^* = 0.5\,\mathrm{nm}$, $\varepsilon_{\mathrm{int}} = \varepsilon = 78$, and all α_i are summarized in table 1. (b) Plot of the reactant concentrations as a function of $c^{\mathrm{b}}_{\mathrm{Na_2CO_3}}$. (c) Plot of the reactant concentrations as a function of $c^{\mathrm{b}}_{\mathrm{NaHCO_3}}$.

Appendix B: Estimate of the surface affinity of carbonate ions to the air interface

In this section we estimate the affinity of carbonate ions to the air-water interface, α_{CO3}, using experimental surface tension data of Na_2CO_3 solutions. Because the carbonate ion, CO_3^{2-}, is divalent, the exact solution of eq. 2 is not available, therefore eq. 2 needs to be solved numerically. Since the solution of Na_2CO_3 is basic, we take the dissociation of water and the reaction of carbonates into account.

Fig. 10a shows the surface tension of Na_2CO_3 and $NaHCO_3$ solutions as a function of their bulk concentration. We do not use the experimental data of Na_2CO_3 taken from Ref. 103 for fitting because they deviate from the other experimental data.[101,102] To obtain the surface affinity of CO_3^{2-}, we calculate the surface tension of Na_2CO_3 solutions by solving the chemical equilibrium equations 8 and 16-18 together with conservation of the total carbon concentration. Here we do not use the reaction eq. 15, because the dissolution of CO_2 from the ambient air into the solution is very slow. If we wait for equilibration of the

reaction described by eq. 15, $NaHCO_3$ and Na_2CO_3 solutions relax and thereby release CO_2. We also neglect the surface excess of neutral molecules CO_2 and H_2CO_3, even though the surface excess of these neutral species enter the surface tension difference, because their bulk concentrations are much smaller than the main cation and anion concentrations in the bulk. We use $\varepsilon = 78$, $T = 298\,\mathrm{K}$, $z^* = 0.5\,\mathrm{nm}$, $\alpha_{\mathrm{Na}} = 1.2$, $\alpha_{\mathrm{H_3O}} = -0.9$, $\alpha_{\mathrm{OH}} = 1.6$, $\alpha_{\mathrm{HCO_3}} = -0.4$.[72] Note that $\alpha_{\mathrm{HCO_3}}$ has been obtained by assuming only the dissociation $NaHCO_3 \rightarrow Na^+ + HCO_3^-$. We obtain $\alpha_{\mathrm{CO_3}} = 1.4$ for the best fit (blue line in Fig. 10a). When we assume only the reaction $Na_2CO_3 \rightarrow 2Na^+ + CO_3^{2-}$, the result is almost the same (orange broken line in Fig. 10a), showing that the reactions, eqs. 8 and 16-18 are not important for the surface tension of Na_2CO_3 solutions in this concentration range.

The red line in Fig. 10a depicts the theoretical surface tension of a $NaHCO_3$ solution considering the chemical equilibrium described by equations 8 and 16-18. Here we also neglect the surface excess of neutral molecules, and we use the same parameters as for the calculation of the Na_2CO_3 surface tension. The light blue broken line in Fig. 10a is the theoretical surface tension of a $NaHCO_3$ solution assuming only $NaHCO_3 \rightarrow Na^+ + HCO_3^-$, which is almost the same as the red solid line. The agreement between the two theoretical lines shows that the surface tension of Na_2CO_3 and $NaHCO_3$ solution can be predicted by treating the solutions as strong electrolytes, neglecting the reactions, eqs. 8 and 16-18.

Figs. 10b and c show the bulk ion concentrations due to the chemical equilibrium eqs. 8 and 16-18 for Na_2CO_3 and $NaHCO_3$ solutions. We find that the dominant ions in Na_2CO_3 solutions at $c^{\mathrm{b}}_{\mathrm{salt}} > 10\,\mathrm{mM}$ are Na^+ and CO_3^{2-} ions, whereas the dominant ions in $NaHCO_3$ solutions at $c^{\mathrm{b}}_{\mathrm{salt}} > 10\,\mathrm{mM}$ are Na^+ and HCO_3^-. These results show that carbonate equilibria in electrolyte are rather complex.

Appendix C: Slip effect on the ζ potential caused by acidic impurities

In this section we examine how slip effects modify the impurity-induced ζ potential. Fig. 11 shows the ζ potential including slip effects in the presence of acidic impurities. The slip length $b = z^*(\eta/\eta_{\rm int} - 1) = 2\,{\rm nm}$ is identical to the slip length found for hydrophobic diamond surfaces in molecular dynamics simulations.[87] Except for $\eta_{\rm int}$, the parameters are the same as those used in Fig. 4.

In Fig. 11a ($c^{\rm b}_{\rm A,tot} = 50\,{\rm nM}$), the effect of the salt concentration on the ζ potential is suppressed compared to the case without slip, shown in Fig. 4a, meaning that the three curves for different salt concentration are very similar to each other. When the impurity concentration is higher ($c^{\rm b}_{\rm A,tot} = 500\,{\rm nM}$, Fig. 11b), the slip effect is even more drastic and the order of the absolute ζ potential with respect to the salt concentration is reversed at basic conditions and thus different from the experimental data and also different from the prediction without slip in Fig. 4b. To linear order in κz^*, the slip effect modifies the ζ potential by the factor $(1 + \kappa b)$,[81,104] which explains the trends seen in Fig. 11a and b. Fig. 11c shows the ζ potential at pH = 7 as a function of $c^{\rm b}_{\rm A,tot}$ and demonstrates the reversal of the salinity dependence for $c^{\rm b}_{\rm A,tot} > 100\,{\rm nM}$ for both ${\rm pK_a} = 5$ and 7.

Fig. 11 demonstrates that the predicted ζ potential differs from the experimental results for finite slip, even though hydrophobic surfaces exhibit a finite slip length.[77] It is at present not clear where this discrepancy comes from, possibly the adsorption of impurities onto the interface modifies the interfacial effective viscosity, as suggested earlier in related works.[77,105–107]

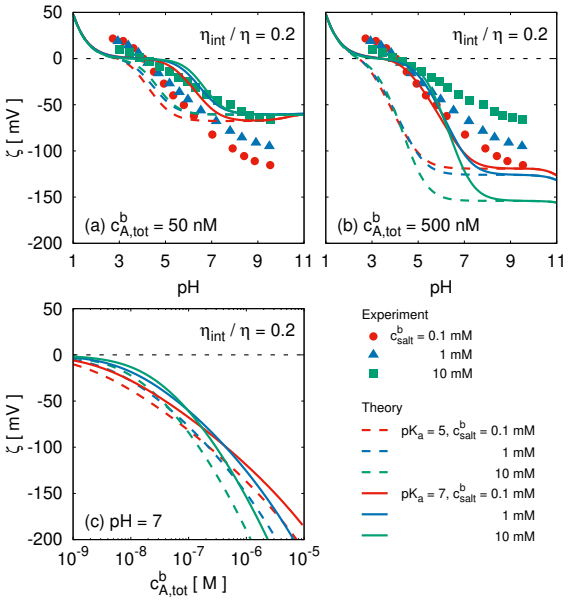

Figure 11: Slip effect on the ζ potential caused by acidic impurities for $\eta_{\rm int}/\eta = 0.2$. Other parameters are the same as those used in Fig. 4. (a,b) ζ potential as a function of pH for $\mathrm{pK_a} = 7$ (solid lines) and for $\mathrm{pK_a} = 5$ (broken lines). (c) ζ potential as a function of $c^{\rm b}_{\rm A,tot}$. The symbols in (a,b) represent the experimental data.[6]

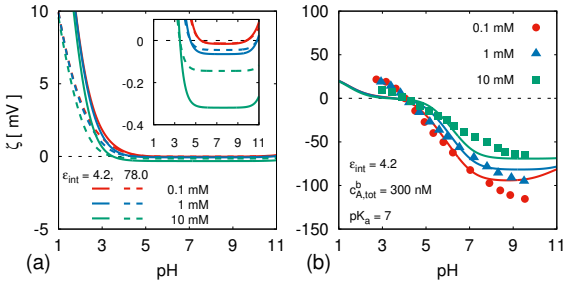

Figure 12: (a) Difference between the ζ potential with and without interfacial dielectric effects. The presence of impurities and carbon dioxide is not considered, and the parameters except for $\varepsilon_{\rm int}$ are the same as those used in Fig. 2. The broken lines are calculated using $\varepsilon_{\rm int} = \varepsilon = 78$, and the solid lines are calculated using $\varepsilon_{\rm int} = 4.2$. The inset shows a magnification. (b) ζ potential predicted for an acidic impurity concentration of $c^{\rm b}_{\rm A,tot} = 300\,\mathrm{nM}$ and $\mathrm{pK_a} = 7$, where $\varepsilon_{\rm int} = 4.2$ is used and all other parameters are the same as those used in Fig. 4b. The symbols represent the experimental data for Teflon surfaces AF.[6]

Appendix D: Effect of interfacial dielectric constant on the ζ potential

In this section, we demonstrate that interfacial dielectric effects are not relevant for the ζ potential of hydrophobic surfaces. Fig. 12a shows the difference between the ζ potential with and without a modified interfacial dielectric constant. Here we do not consider impurities or carbon dioxide dissolution, and the parameters except for $\varepsilon_{\mathrm{int}}$ are the same as those used in Fig. 2. The broken lines are calculated using $\varepsilon_{\mathrm{int}} = \varepsilon = 78$, and the solid lines are calculated using $\varepsilon_{\mathrm{int}} = 4.2$, which is an estimate based on the interfacial capacitance of a hydrophobe-water interface from molecular dynamics simulation.[86] The difference between the results for the two scenarios is very small, we thus conclude that dielectric interfacial effects cannot explain the experimental ζ potential without the presence of impurities.

Fig. 12b shows the ζ potential predicted in the presence of acidic impurities for $c^{\mathrm{b}}_{\mathrm{A,tot}} = 300\,\mathrm{nM}$ and $\mathrm{pK_a} = 7$, where $\varepsilon_{\mathrm{int}} = 4.2$ is used and other parameters are the same as those used in Fig. 4b. The fitted impurity concentration 300 nM is smaller than 500 nM used in Fig. 4b, which is caused by the presence of the modified interfacial dielectric constant, but this difference is not rather marginal.

Acknowledgement

Funding by the Deutsche Forschungsgemeinschaft (DFG) via grant NE810/11 is gratefully acknowledged. YU was supported by JSPS Overseas Research Fellowships No. 201860001.

References

(1) Israelachvili, J. N. *Intermolecular and Surface Forces*, 3rd ed.; Elsevier, 2011.

(2) Russel, W. B.; Saville, D. A.; Schowalter, W. R. *Colloidal Dispersions*; Cambridge University Press: Cambridge, 1989.

(3) Scales, P. J.; Grieser, F.; Healy, T. W.; White, L. R.; Chan, D. Y. C. Electrokinetics of the silica-solution interface: a flat plate streaming potential study. *Langmuir* **1992**, *8*, 965–974.

(4) Wiese, G. R.; Healy, T. W. Adsorption of Al(III) at the TiO_2/H_2O Interface. *J. Colloid Int. Sci.* **1975**, *51*, 434–452.

(5) Trefalt, G.; Behrens, S. H.; Borkovec, M. Charge Regulation in the Electrical Double Layer: Ion Adsorption and Surface Interactions. *Langmuir* **2016**, *32*, 380–400.

(6) Zimmermann, R.; Dukhin, S.; Werner, C. Electrokinetic Measurements Reveal Interfacial Charge at Polymer Films Caused by Simple Electrolyte Ions. *J. Phys. Chem. B* **2001**, *105*, 8544–8549.

(7) Matjević, S. K. E. Stability of carbon suspensions. *Colloids and Surfaces* **1982**, *5*, 179–186.

(8) Lau, A. C.; Furlong, D. N.; Healy, T. W.; F.Grieser, The electrokinetic properties of carbon black and graphitized carbon black aqueous colloids. *Colloids and Surfaces* **1986**, *18*, 93–104.

(9) Miller, S. A.; Young, V. Y.; Martin, C. R. Electroosmotic Flow in Template-Prepared Carbon Nanotube Membranes. *J. Am. Chem. Soc.* **2001**, *123*, 12335–12342.

(10) Härtl, A.; Garrido, J. A.; Nowy, S.; Zimmermann, R.; Horinek, C. W. D.; Netz, R.; Stutzmann, M. The Ion Sensitivity of Surface Conductive Single Crystalline Diamond. *J. Am. Chem. Soc.* **2007**, *129*, 1287–1292.

(11) Siria, A.; Poncharal, P.; Biance, A.-L.; Fulcrand, R.; Blase, X.; Purcell, S. T.; Bocquet, L. Giant osmotic energy conversion measured in a single transmembrane boron nitride nanotube. *Nature* **2013**, *494*, 455–458.

(12) Chander, S.; Fuerstenau, D. W. On the Natural Floatability of Molybdenite. *Society of Mining Engineers, AIME* **1972**, *252*, 62–69.

(13) Derjaguin, B. V.; Dukhin, S. S. Theory of flotation of small and medium-size particles. *Progress in Surface Science* **1993**, *43*, 241–266.

(14) Derjaguin, B. V.; Shukakidse, N. D. Dependence of the floatability of antimonite on the value of zeta-potential. *Progress in Surface Science* **1993**, *43*, 267–272.

(15) Fullston, D.; Fornasiero, D.; Ralston, J. Zeta potential study of the oxidation of copper sulfide minerals. *Colloids and Surfaces A: Physicochemical and Engineering Aspects* **1999**, *146*, 113–121.

(16) Kallay, N.; Preocănin, T.; Šupljika, F.; Lützenkirchen, J.; Lovković, M. Influence of interfacial water layer on surface properties of silver halides: Effect of pH on the isoelectric point. *Journal of Colloid and Interface Science* **2012**, *375*, 167–171.

(17) Selmani, A.; Lützenkirchen, J.; Kallay, N.; Preočanin, T. Surface and zeta-potentials of silver halide single crystals: pH-dependence in comparison to particle systems. *J. Phys.: Condens. Matter* **2014**, *26*, 244104.

(18) Healy, T. W.; Fuerstenau, D. W. The isoelectric point/point-of zero-charge of interfaces formed by aqueous solutions and nonpolar solids, liquids, and gases. *Journal of Colloid and Interface Science* **2007**, *309*, 183–188.

(19) Billett, D. F.; Hough, D. B.; Ottewill, R. H. Studies on the Contact Angle of the Charged Silver Iodide-Solution-Vapour Interface. *J. Electroanal. Chem.* **1976**, *74*, 107–120.

(20) Kozbial, A.; Trouba, C.; Liu, H.; Li, L. Characterization of the Intrinsic Water Wettability of Graphite Using Contact Angle Measurements: Effect of Defects on Static and Dynamic Contact Angles. *Langmuir* **2017**, *33*, 959–967.

(21) Usui, S.; Sasaki, H. Zeta potential measurements of bubbles in aqueous surfactant solutions. *Journal of Colloid and Interface Science* **1978**, *65*, 36–45.

(22) Usui, S.; Sasaki, H.; Matsukawa, H. The dependence of zeta potential on bubble size as determined by the dorn effect. *Journal of Colloid and Interface Science* **1981**, *81*, 80–84.

(23) Brandon, N. P.; Kelsall, G. H.; Levine, S.; Smith, A. L. Interfacial electrical properties of electrogenerated bubbles. *J. Appl. Electrochem.* **1985**, *15*, 485–493.

(24) Yoon, R.-H.; Yordan, J. L. Zeta-potential measurements on microbubbles generated using various surfactants. *Journal of Colloid and Interface Science* **1986**, *113*, 430–438.

(25) Laskowski, J. S.; Yordan, J. L.; Yoon, R. H. Electrokinetic potential of microbubbles generated in aqueous solutions of weak electrolyte type surfactants. *Langmuir* **1989**, *5*, 373–376.

(26) Li, C.; Somasundaran, P. Reversal of bubble charge in multivalent inorganic salt solutions-Effect of magnesium. *Journal of Colloid and Interface Science* **1991**, *146*, 215–218.

(27) Li, C.; Somasundaran, P. Reversal of bubble charge in multivalent inorganic salt solutions-Effect of aluminum. *Journal of Colloid and Interface Science* **1992**, *148*, 587–591.

(28) Li, C.; Somasundaran, P. Reversal of bubble charge in multivalent inorganic salt solutions-Effect of lanthanum. *Colloids and Surfaces A* **1993**, *81*, 13–15.

(29) Kelsall, G. H.; Tang, S.; Smith, A. L.; Yurdakul, S. Measurement of rise and electrophoretic velocities of gas bubbles. *J. Chem. Soc. Faraday Trans.* **1996**, *92*, 3879–3885.

(30) Kelsall, G. H.; Tang, S.; Yurdakul, S.; Smith, A. L. Electrophoretic behaviour of bubbles in aqueous electrolytes. *J. Chem. Soc. Faraday Trans.* **1996**, *92*, 3887–3893.

(31) Yang, C.; Dabros, T.; Li, D.; Czarnecki, J.; Masliyah, J. H. Measurement of the Zeta Potential of Gas Bubbles in Aqueous Solutions by Microelectrophoresis Method. *Journal of Colloid and Interface Science* **2001**, *243*, 128–135.

(32) Takahashi, M. Potential of Microbubbles in Aqueous Solutions: Electrical Properties of the Gas-Water Interface. *J. Phys. Chem. B* **2005**, *109*, 21858–21864.

(33) Najafi, A. S.; Drelich, J.; Yeung, A.; Xu, Z.; Masliyah, J. A novel method of measuring electrophoretic mobility of gas bubbles. *Journal of Colloid and Interface Science* **2007**, *308*, 344–350.

(34) Oliveira, C.; Rubio, J. Zeta potential of single and polymer-coated microbubbles using an adapted microelectrophoresis technique. *International Journal of Mineral Processing* **2011**, *98*, 118–123.

(35) Calgaroto, S.; Wilberg, K.; Rubio, J. On the nanobubbles interfacial properties and future applications in flotation. *Minerals Engineering* **2014**, *60*, 33–40.

(36) Alty, T.; Johnson, O. The cataphoresis of particles of the fatty acids and related compounds. *The London, Edinburgh, and Dublin Philosophical Magazine and Journal of Science* **1935**, *20*, 129–145.

(37) Carruthers, J. C. The electrophoresis of certain hydrocarbons and their simple derivatives as a function of pH. *Trans. Faraday Soc.* **1938**, *34*, 300–307.

(38) Dickinson, W. The effect of pH upon the electrophoretic mobility of emulsions of certain hydrocarbons and aliphatic halides. *Trans. Faraday Soc.* **1941**, *37*, 140–148.

(39) Taylor, A. J.; Wood, F. W. The electrophoresis of hydrocarbon droplets in dilute solutions of electrolytes. *Trans. Faraday Soc.* **1957**, *53*, 523–529.

(40) Haydon, D. A. A Study of the Relation Between Electrokinetic Potential and Surface Charge Density. *Proc. R. Soc. Lond. A* **1960**, *258*, 319–328.

(41) Stachurski, J.; Michałek, M. The Effect of the ζ Potential on the Stability of a Non-Polar Oil-in-Water Emulsion. *J. Colloid Interface Sci.* **1996**, *184*, 433–436.

(42) Marinova, K. G.; Alargova, R. G.; Denkov, N. D.; Velev, O. D.; Petsev, D. N.; Ivanov, I. B.; Borwankar, R. P. Charging of Oil-Water Interfaces Due to Spontaneous Adsorption of Hydroxyl Ions. *Langmuir* **1996**, *12*, 2045–2051.

(43) Jabloński, J.; Janusz, W.; Szczypa, J. Adsorption Properties of the stearic acid octadecane particles in aqueous solutions. *Journal of Dispersion Science and Technology* **1999**, *20*, 165–175.

(44) Wuzhang, J.; Song, Y.; Sun, R.; Pan, X.; Li, D. Electrophoretic mobility of oil droplets in electrolyte and surfactant solutions. *Electrophoresis* **2015**, *36*, 2489–2497.

(45) Yang, F.; Wu, W.; Chen, S.; Gan, W. The ionic strength dependent zeta potential at the surface of hexadecane droplets in water and the corresponding interfacial adsorption of surfactants. *Soft Matter* **2017**, *13*, 638–646.

(46) Roger, K.; Cabane, B. Why Are Hydrophobic/Water Interfaces Negatively Charged? *Angew. Chem. Int. Ed.* **2012**, *51*, 5625–5628.

(47) Vaćha, R.; Marsalek, O.; Willard, A. P.; Bonthuis, D. J.; R.Netz, R.; Jungwirth, P. Charge Transfer between Water Molecules As the Possible Origin of the Observed Charging at the Surface of Pure Water. *J. Phys. Chem. Lett.* **2012**, *3*, 107–111.

(48) Yan, X.; Delgado, M.; Aubry, J.; Gribelin, O.; Stocco, A.; Cruz, F. B.-D.; Bernard, J.; Ganachaud, F. Central role of bicarbonate anions in charging water/hydrophobic interfaces. *J. Phys. Chem. Lett.* **2018**, *9*, 96–103.

(49) Uematsu, Y.; Bonthuis, D. J.; Netz, R. R. Impurity effects at hydrophobic surfaces. *Current Opinion in Electrochemistry* **2019**, *13*, 166–173.

(50) Lützenkirchen, J.; Preočanin, T.; Kallay, N. A macroscopic water structure based model for describing charging phenomena at inert hydrophobic surfaces in aqueous electrolyte solutions. *Phys. Chem. Chem. Phys.* **2008**, *10*, 4946–4955.

(51) Beattie, J. K.; Gray-Weale, A. Oil/Water Interface Charged by Hydroxide Ions and Deprotonated Fatty Acids: A Comment. *Angew. Chem. Int. Ed.* **2012**, *51*, 12941–12942.

(52) Jena, K. C.; Scheu, R.; Roke, S. Surface Impurities Are Not Responsible For the Charge on the Oil/Water Interface: A Comment. *Angew. Chem. Int. Ed.* **2012**, *51*, 12938–12940.

(53) Grosjean, B.; Pean, C.; Siria, A.; Bocquet, L.; Vuilleumier, R.; Bocquet, M.-L. Chemisorption of Hydroxide on 2D Materials from DFT Calculations: Graphene versus Hexagonal Boron Nitride. *J. Phys. Chem. Lett.* **2016**, *7*, 4695–4700.

(54) Grosjean, B.; Bocquet, M.-L.; Vuilleumier, R. Versatile electrification of two-dimensional nanomaterials in water. *Nat Commun.* **2019**, *10*, 1656.

(55) Kudin, K. N.; Car, R. Why Are Water-Hydrophobic Interfaces Charged? *J. Am. Chem. Soc.* **2008**, *130*, 3915–3919.

(56) Mundy, C. J.; Kuo, I.-F. W.; Tuckerman, M. E.; Lee, H.-S.; Tobias, D. J. Hydroxide anion at the air/water interface. *Chem. Phys. Lett.* **2009**, *481*, 2–8.

(57) Tian, C. S.; Shen, Y. R. Structure and charging of hydrophobic material/water interfaces studied by phase-sensitive sum-frequency vibrational spectroscopy. *Proc. Nat. Acad. Sci. United States Am.* **2009**, *106*, 15148–15153.

(58) Mamatkulov, S. I.; Allolio, C.; Netz, R. R.; Bonthuis, D. J. Orientation-Induced Adsorption of Hydrated Protons at the Air-Water Interface. *Angew. Chem. Int. Ed.* **2017**, *56*, 15846–15851.

(59) Duignan, T. T.; Parsons, D. F.; Ninham, B. W. Hydronium and hydroxide at the air-water interface with a continuum solvent model. *Chem. Phys. Lett.* **2015**, *635*, 1–12.

(60) Tse, Y.-L. S.; Chen, C.; Lindberg, G. E.; Kumar, R.; Voth, G. A. Propensity of Hydrated Excess Protons and Hydroxide Anions for the Air-water Interface. *J. Am. Chem. Soc.* **2015**, *137*, 12610–12616.

(61) P. B, P.; Saykally, R. J. Evidence for an enhanced hydronium concentration at the liquid water surface. *J. Phys. Chem. B* **2005**, *109*, 7976–7980.

(62) Matyushov, D. V. Electrophoretic mobility without charge driven by polarisation of the nanoparticle-water interface. *Molecular Physics* **2014**, *112*, 2029–2039.

(63) Poli, E.; Jong, K. H.; Hassanali, A. Charge Transfer as a Ubiquitous Mechanism in Determining the Negative Charge at Hydrophobic Interfaces. *arXiv:1904.05766 [physics.chem-ph]* **2019**,

(64) Roger, K.; Cabane, B. Uncontaminated Hydrophobic/Water Interfaces Are Uncharged: A Reply. *Angew. Chem. Int. Ed.* **2012**, *51*, 12943–12945.

(65) von Smoluchowski, M. Versuch einer Mathematischen Theorie der Kiagulationskinetik Kolloider Lösungen. *Z. Phys. Chem.* **1918**, *92*, 129–168.

(66) Hückel, E. Die Kataphorese der Kugel. *Physik. Z.* **1924**, *25*, 204.

(67) Henry, D. C. The Cataphoresis of Suspended Particles. Part I. The Equation of Cataphoresis. *Proc. R. Soc. London, Ser. A* **1931**, *133*, 106.

(68) O'Brien, L. R.; White, L. R. Electrophoretic Mobility of a Spherical Colloidal Particle. *J. Chem. Soc., Faraday Trans. 2* **1978**, *74*, 1607–1626.

(69) Ohshima, H.; Healy, T. W.; White, L. R. Electrokinetic phenomena in a dilute suspension of charged mercury drops. *J. Chem. Soc. Faraday Trans. 2* **1984**, *80*, 1643–1667.

(70) Baygents, J. C.; Saville, D. A. Electrophoresis of drops and bubbles. *J. Chem. Soc. Faraday Trans.* **1991**, *87*, 1883–1898.

(71) Schnitzer, O.; Frankel, I.; Yariv, E. Electrophoresis of bubbles. *J. Fluid Mech.* **2014**, *753*, 49–79.

(72) Uematsu, Y.; Bonthuis, D. J.; Netz, R. R. Surface-active charged impurities at nanomolar concentration induce Jones-Ray effect. *J. Phys. Chem. Lett.* **2018**, *9*, 189–193.

(73) Uematsu, Y.; Chida, K.; Matsubara, H. Intentionally Added Ionic Surfactants Induce Jones-Ray Effect at Air-Water Interface. *Colloid and Interface Science Communications* **2018**, *27*, 45–48.

(74) Schelero, N.; von Klitzing, R. Correlation between specific ion adsorption at the air/water interface and long-range interactions in colloidal systems. *Soft Matter* **2011**, *7*, 2936–2942.

(75) Parkinson, L.; Sedev, R.; Fornasiero, D.; Ralston, J. The terminal rise velocity of 10-100 μm diameter bubbles in water. *Journal of Colloid and Interface Science* **2008**, *322*, 168–172.

(76) Henry, C. L.; Parkinson, L.; Ralston, J. R.; Craig, V. S. J. A Mobile Gas-Water Interface in Electrolyte Solutions. *J. Phys. Chem. C* **2008**, *112*, 15094–15097.

(77) Manor, O.; Vakarelski, I. U.; Stevens, G. W.; Grieser, F.; Dagastine, R. R.; Chan, D. Y. C. Dynamic Forces between Bubbles and Surfaces and Hydrodynamic Boundary Conditions. *Langmuir* **2008**, *24*, 11533–11543.

(78) Maali, A.; Boisgard, R.; Chraibi, H.; Zhang, Z.; Kellay, H.; Würger, A. Viscoelastic Drag Forces and Crossover from No-Slip to Slip Boundary Conditions for Flow near Air-Water Interfaces. *Phys. Rev. Lett.* **2017**, *118*, 084501.

(79) Osakai, T.; Ebina, K. Non-Bornian Theory of the Gibbs Energy of Ion Transfer between Two Immiscible Liquids. *J. Phys. Chem. B* **1998**, *102*, 5691–5698.

(80) Hirsikko, A. et al. Atmospheric ions and nucleation: a review of observations. *Atmos. Chem. Phys.* **2011**, *11*, 767–798.

(81) Uematsu, Y.; Netz, R. R.; Bonthuis, D. J. Analytical interfacial layer model for the capacitance and electrokinetics of charged aqueous interfaces. *Langmuir* **2018**, *34*, 90979113.

(82) Bonthuis, D. J.; Netz, R. R. Unraveling the Combined Effects of Dielectric and Viscosity Profiles on Surface Capacitance, Electro-Osmotic Mobility, and Electric Surface Conductivity. *Langmuir* **2012**, *28*, 16049–16059.

(83) Langmuir, I. The Adsorption of Gases on Plane Surfaces of Glass, Mica and Platinum. *J. Am. Chem. Soc.* **1918**, *40*, 1361–1403.

(84) Bocquet, L.; Charlaix, E. Nanofluidics, from bulk to interfaces. *Chem. Soc. Rev.* **2010**, *39*, 1073–1095.

(85) Persat, A.; Chambers, R. D.; Santiago, J. G. Basic principles of electrolyte chemistry for microfluidic electrokinetics. Part I: Acid/base equilibria and pH buffers. *Lab on a Chip* **2009**, *9*, 2437–2453.

(86) Bonthuis, D. J.; Gekle, S.; Netz, R. R. Dielectric Profile of Interfacial Water and its Effect on Double-Layer Capacitance. *Phys. Rev. Lett.* **2011**, *107*, 166102.

(87) Sendner, C.; Horinek, D.; Bocquet, L.; Netz, R. R. Interfacial water at hydrophobic and hydrophilic surfaces: slip, viscosity, and diffusion. *Langmuir* **2009**, *25*, 10768–10781.

(88) Horinek, D.; Herz, A.; Vrbka, L.; Sedlmeier, F.; Mamatkulov, S. I.; Netz, R. R. Specific ion adsorption at the air/water interface: The role of hydrophobic solvation. *Chem. Phys. Lett.* **2009**, *479*, 173–183.

(89) Huang, D. M.; Sendner, C.; Horinek, D.; Netz, R. R.; Bocquet, L. Water Slippage versus Contact Angle: A Quasiuniversal Relationship. *Phys. Rev. Lett.* **2008**, *101*, 226101.

(90) Lide, D. R., Ed. *CRC Handbook of Chemistry and Physics*, 84th ed.; CRC Press, 2004.

(91) Netz, R. R. Charge regulation of weak polyelectrolytes at low- and high-dielectric-constant substrates. *J. Phys.: Condens. Matter* **2003**, *15*, S239S244.

(92) Gabler, R.; Hegde, R.; Hughes, D. Degradation of High Purity Water on Storage. *Journal of Liquid Chromatography* **1983**, *6*, 2565–2570.

(93) Kuroki, Y. Influence of Impurities in Ultra-Pure Water on Ultratrace Analyses with Analytical Instruments. *Bunseki Kagaku (in Japanese)* **2010**, *59*, 85–93.

(94) Regnault, C.; Kano, I.; Darbouret, D.; Mabic, S. Ultrapure water for liquid chromatographymass spectrometry studies. *Journal of Chromatography A* **2004**, *1030*, 289–295.

(95) Herath, H. M. D. R.; Shaw, P. N.; Cabot, P.; Hewavitharana, A. K. Effect of ionization suppression by trace impurities in mobile phase water on the accuracy of quantification by high-performance liquid chromatography/mass spectrometry. *Rapid Commun. Mass Spectrom.* **2010**, *24*, 1502–1506.

(96) Roger, K.; Eissa, M.; Elaissari, A.; Cabane, B. Surface Charge of Polymer Particles in Water: The Role of Ionic End- Groups. *Langmuir* **2013**, *29*, 11244–11250.

(97) Wells, C. F. Acid-Base Equilibria in Dilute Aqueous Alcohols containing Mineral Acids. *Nature* **1962**, *196*, 770–771.

(98) Giles, G. D.; Wells, C. F. Acid-base Equilibria involving Oxygen-containing Molecules in Dilute Aqueous Solution. *Nature* **1964**, *201*, 606–607.

(99) Lee, D. G.; Sadar, M. H. The basicity of aliphatic carboxylic acids. *Canadian Journal of Chemistry* **1976**, *54*, 3464–3469.

(100) Wiersema, P. H.; Loeb, A. L.; Overbeek, J. T. G. Calculation of the Electrophoretic Mobility of a Spherical Colloid Particle. *J. Colloid Interface Sci.* **1966**, *22*, 78–99.

(101) Washburn, E. W., Ed. *International Critical Tables of Numerical Data, Physics, Chemistry, and Technology*, 1st ed.; Knovel: Norwich, NY, 1930; Vol. IV; pp 463–466.

(102) Matubayasi, N. *Surface tension and related thermodynamic quantities of aqueous electrolyte solutions*; CRC Press, 2014.

(103) Ozdemir, O.; Karakashev, S. I.; Nguyen, A. V.; Miller, J. D. Adsorption of carbonate and bicarbonate salts at the air-brine interface. *Int. J. Miner. Process.* **2006**, *81*, 149–158.

(104) Barrat, J.; Bocquet, L. Large slip effect at a nonwetting fluidsolid interface. *Phys. Rev. Lett.* **1999**, *82*, 4671–4674.

(105) Joly, L.; Detcheverry, F.; Biance, A.-L. Anomalous ζ Potential in Foam Films. *Phys. Rev. Lett.* **2014**, *113*, 088301.

(106) Lima, A. B. D.; Joly, L. Electro-osmosis at surfactant-laden liquidgas interfaces: beyond standard models. *Soft Matter* **2017**, *13*, 3341.

(107) Blanc, B.; Bonhomme, O.; Brevet, P.-F.; Benichou, E.; Ybert, C.; Biance, A.-L. Electroosmosis near surfactant laden liquid-air interfaces. *Soft Matter* **2018**, *14*, 2604–2609.

Graphical TOC Entry